Multidisciplinary Research Journal
ISSN: 3049-2718 (Print)

Volume 1, Issue 2, 2025
April – June 2025

*Research Article*

# Predictive Control Based MPPT for Solar Boost Converters to Optimize Performance Under Fluctuating Irradiation and Loads

**Muzammill Ahmed [1]***

[1] School of Electrical and Computer Sciences, Indian Institute of Technology Bhubaneswar, 752050, Odisha, India
* Correspondence: ahmedmuzammil024@gmail.com

Scopus Author ID 57213795113

**Received: 1 February 2025; Accepted: 11 April 2025; Published: 28 April 2025**

**Abstract:** In this study, a hybrid maximum power point tracking (MPPT) approach is proposed by integrating a Current Tracking Perturb and Observe (CT-P&O) algorithm with Finite Control Set Model Predictive Control (FCS-MPC) for solar photovoltaic (PV) fed boost converters. The method aims to improve MPPT accuracy, transient performance, and efficiency under dynamically varying irradiance and load conditions. The CT-P&O algorithm generates a reference current for FCS-MPC, while an enhanced cost function is designed to minimize inductor ripple and ensure smooth converter operation. Unlike conventional approaches that focus solely on resistive loads, the proposed system is validated under both resistive and resistive-inductive (RL) loading, as well as step load changes and irradiance fluctuations. Simulation results in MATLAB/Simulink demonstrate high tracking accuracy, ripple minimization, and robustness, achieving a peak efficiency of 97.8%. The proposed control strategy offers a practical solution for real-world PV applications demanding high performance under uncertain operating conditions.

**Keywords:** Photovoltaic systems; MPPT; Finite Control Set Model Predictive Control (FCS-MPC); P&O algorithm; Ripple minimization; Dynamic load; Solar energy

## 1. Introduction

The rising global energy demand has intensified the shift toward renewable energy sources, with solar photovoltaic (PV) systems emerging as a leading solution due to their sustainability, wide availability, and declining cost [1]. However, despite their advantages, PV systems face inherent challenges such as intermittency and fluctuations in solar irradiance, which directly affect the consistency and efficiency of power output. To address this, extensive research has focused on developing effective Maximum Power Point Tracking (MPPT) algorithms that enable PV systems to operate at their peak power under varying environmental conditions [2].

Among various MPPT techniques, the Perturb and Observe (P&O) algorithm is one of the most widely adopted due to its simplicity and ease of implementation [3]. However, it suffers from significant drawbacks, including slow dynamic response, oscillations around the maximum power point, and reduced efficiency during transient events [4]. In recent years, Model Predictive Control (MPC) has gained attention for power converter applications due to its predictive capabilities and rapid response. In particular, the Finite Control Set MPC (FCS-MPC) variant offers advantages such as eliminating the need for a separate modulator and enabling faster switching decisions [5] [6]. A typical structure of an MPC-based controller is shown in Figure 1. Nevertheless, conventional implementations of MPC often focus solely on

current tracking and are rarely integrated with MPPT strategies. In addition, most studies validate their controllers only under resistive loads, which do not reflect the complex and dynamic nature of real-world applications.

In this study, we propose a novel hybrid MPPT control strategy that combines the simplicity of the Current Tracking P&O (CT-P&O) algorithm with the dynamic performance of FCS-MPC. In our approach, CT-P&O generates a reference current that guides the predictive controller, enhancing tracking accuracy while retaining fast transient response. Furthermore, the proposed FCS-MPC scheme incorporates an improved cost function that includes a ripple-penalizing term to reduce inductor current fluctuations. This not only improves system performance under dynamic load and irradiance changes but also contributes to smoother operation and better power quality.

A key contribution of this work is the validation of the controller under both resistive and resistive-inductive (RL) loads, mimicking real-life scenarios such as motor startups or industrial load switching. While some previous studies have attempted to combine MPPT and predictive control [10], they often overlook the impact of non-linear or dynamically changing loads, and rarely assess system behavior under transient conditions.

The proposed method aims to overcome these limitations by offering a more comprehensive and robust control strategy for PV-fed boost converters. Through simulation and analysis, we demonstrate improved MPPT performance, reduced ripple, and high efficiency—even during sudden changes in load or solar irradiance. This makes the proposed controller highly suitable for real-world deployment in solar energy systems.

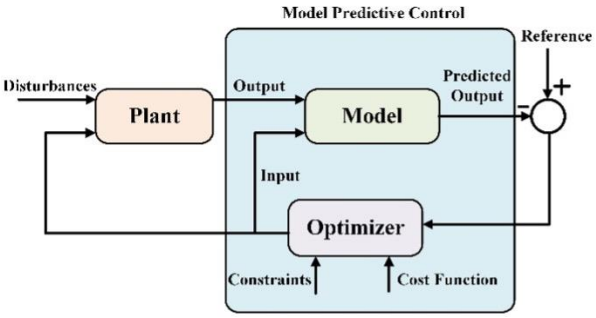


**Figure 1**. Block diagram of Model Predictive Control

## 2. System Description

Figure 2 provides a detailed schematic representation of the proposed photovoltaic power conversion system using Current Tracking Perturb & Observe (CT-P&O) integrated with Finite Control Set Model Predictive Control (FCS-MPC). The system integrates a boost converter, which is fed through the PV module to regulate continuous power flow. The proposed control strategy ensures that the PV system operates at peak power while maintaining a constant input voltage to the boost converter and maximum power extraction from the PV source. The MPPT tracker utilizes the PV voltage and current as the input to execute a current tracking Perturb and Observe (P&O) algorithm, which makes changes accordingly to operate in MPP. The MPP tracker generates a reference current which serves as input to the Finite Control Set Model Predictive Controller (FCS-MPC) block. The FCS-MPC block takes the inductor current, input voltage and output voltage as the inputs to optimize the pre-defined cost

function. The cost function is optimized at each interval and the FCS-MPC determines switching states ensuring efficient operation of the converter.

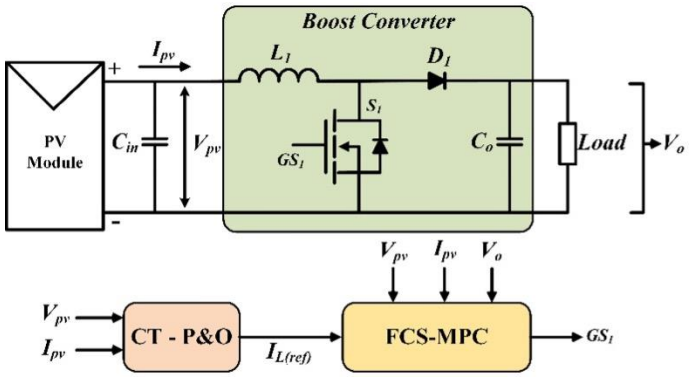


**Figure 2.** Basic structure of the control strategy

## 3. Proposed Methodology

### *3.1. PV System Configuration*

Figure 3 represents a classical model of a single solar cell. The numerical equations that governs the solar cell is given by Equations (1) and (2).

$$I_d = I_o \left[ exp\left(\frac{V_d}{V_T}\right) - 1 \right] \quad (1)$$

$$V_T = \frac{kT}{q} \times nI \times N_{cell} \quad (2)$$

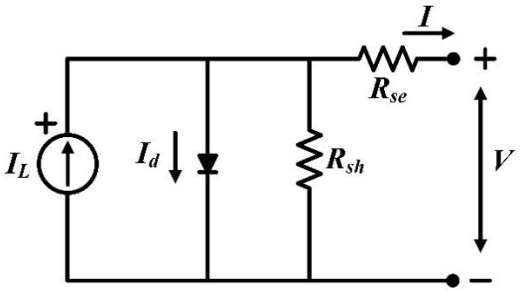

**Figure 3.** Classical model of a PV cell

### *3.2 Boost Converter Operation*

Figure 4 depicts the basic circuit diagram of a Boost Converter. The ON and OFF states are represented in Figure 5 (a) & (b) respectively. The process of energy absorption and injection constitute of an entire switching cycle. When the switch S1 is ON, the current flows through the inductor and stores energy in the inductor. When S1 is OFF, the current would now be flowing through the inductor, diode and load. During this period the energy of the inductor keeps on falling until the next cycle begins.

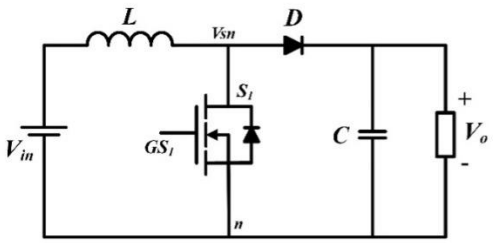


**Figure 4.** Boost Converter

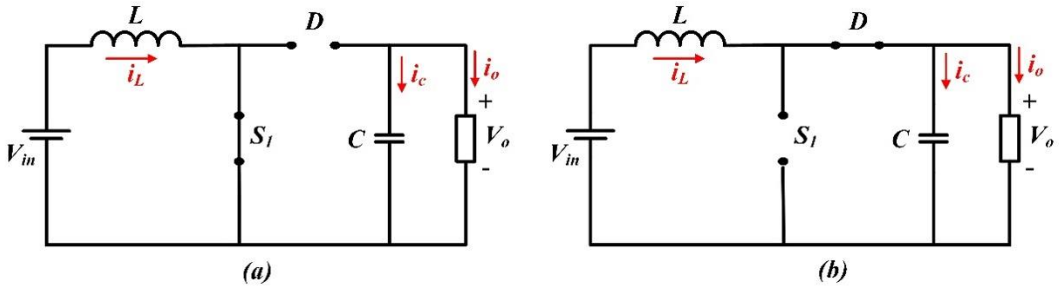


**Figure 5.** Boost Converter (a) S1 is ON (b) S1 is OFF

When $S_1$ is ON:

$$V_L = L\frac{di_L}{dt} = V_{in} - i_L r_L \tag{3}$$

$$\frac{di_L}{dt} = \frac{V_{in}}{L} - \frac{i_L r_L}{L} \tag{4}$$

$$i_C = -i_O \tag{5}$$

$$\frac{dV_o}{dt} = -\frac{V_O}{RC} \tag{6}$$

When $S_1$ is OFF:

$$V_L = L\frac{di_L}{dt} = V_{in} - i_L r_L - V_O \tag{7}$$

$$\frac{di_L}{dt} = \frac{V_{in}}{L} - \frac{i_L r_L}{L} - \frac{V_O}{L} \tag{8}$$

$$i_L = i_C + i_O \tag{9}$$

$$\frac{dV_o}{dt} = \frac{i_L}{C} - \frac{V_O}{RC} \tag{10}$$

where $r_L$ is the DC equivalent resistance in case of an inductor. $i_L$ and $V_o$ are the state variables for the boost converter.

### *3.3 Model Predictive Control modelling*

The predictive control design involves a series of systematic approach in order to improve the performance and effectiveness of the system. MPC utilizes the system model and real time decision making in order to predict the future values to provide precise control of the

converter. In order to use the system modelling to design the model preditive control it is important that the parameters are converted to discrete domain. Another important factor during the designing of MPC is the instances at which the signals are sampled. Incorrect sampling will result in wrong prediction of the future values thus giving wrong prediction. In the proposed scheme Finite Control Set Model Predictive Control (FCS-MPC) is used to leverage gating signal of switch. This architecture reduces the need of using a modulator to generate the pulses for the switch. A single step prediction horizon chosen to reduce compuational burden of controller.

*3.3.1 Selection of the prediction parameters*

The control logic for the proposed architecture is designed by discretizing the model Equations (3), (5), (7) and (9) using Euler's approximations to provide the closest approximations between the continuous and discrete values.

$$\frac{dz(t)}{dt} \approx \frac{z(T+1)-z(T)}{T_s} \tag{11}$$

where T is the sampling instant and Ts is the sampling period.
When S1 is ON and using Equations (4) & (6),

$$\frac{di_L}{dt} = \frac{V_{in}}{L} - \frac{i_L r_L}{L} \tag{12}$$

$$\frac{\Delta i_L}{\Delta t} = \frac{V_{in}}{L} - \frac{i_L r_L}{L} \tag{13}$$

$$\frac{i_L(k+1)- i_L(k)}{T_s} = \frac{V_{in}(k)}{L} - \frac{i_L(k) r_L}{L} \tag{14}$$

$$i_L(k+1) = i_L(k) + \frac{V_{in}(k)}{L} T_s - \frac{i_L(k) r_L}{L} T_s \tag{15}$$

As $V_{in} = V_{pv}$ for our case we can replace $V_{in}$ in Equation (15) as $V_{pv}$,

$$i_L(k+1) = i_L(k) + \frac{V_{pv}(k)}{L} T_s - \frac{i_L(k) r_L}{L} T_s \tag{16}$$

$$\frac{dV_o}{dt} = -\frac{V_O}{RC} \tag{17}$$

$$\frac{\Delta V_o}{\Delta t} = -\frac{V_O}{RC} \tag{18}$$

$$\frac{V_o(k+1)- V_o(k)}{T_s} = -\frac{V_O(k)}{RC} \tag{19}$$

$$V_o(k+1) = V_o(k) - \frac{V_O(k)}{RC} T_s = V_o(k)\left\{1 - \frac{T_s}{RC}\right\} \tag{20}$$

When $S_1$ is OFF and using Equations (8) & (10),

$$\frac{di_L}{dt} = \frac{V_{in}}{L} - \frac{i_L r_L}{L} - \frac{V_O}{L} \tag{21}$$

$$\frac{\Delta i_L}{\Delta t} = \frac{V_{in}}{L} - \frac{i_L r_L}{L} - \frac{V_o}{L} \tag{22}$$

$$\frac{i_L(k+1) - i_L(k)}{T_s} = \frac{V_{in}(k)}{L} - \frac{i_L(k) r_L}{L} - \frac{V_o(k)}{L} \tag{23}$$

$$i_L(k+1) = i_L(k) + \frac{V_{pv}(k)}{L} T_s - \frac{i_L(k) r_L}{L} T_s - \frac{V_o(k)}{L} T_s \tag{24}$$

$$\frac{dV_o}{dt} = \frac{i_L}{C} - \frac{V_O}{RC} \tag{25}$$

$$\frac{\Delta V_o}{\Delta t} = \frac{i_L}{C} - \frac{V_O}{RC} \tag{26}$$

$$\frac{V_o(k+1) - V_o(k)}{T_s} = \frac{i_L(k)}{C} - \frac{V_o(k)}{RC} \tag{27}$$

$$V_o(k+1) = V_o(k) + \frac{i_L(k)}{C} T_s - \frac{V_o(k)}{RC} T_s \tag{28}$$

The predicted values of the inductor current during ON and OFF duration of the switch are decided by Equations (16) & (24) respectively by iterating over a particular set of states. The capacitor voltages is predicted using the model as described in Equations (20) & (28) during ON & OFF states respectively.

*3.3.2 Design of the Cost Function*

The cost function selection is vital in MPC as it influences controller's performance, stability and robustness. The cost function helps in optimizing the control actions over a particular prediction horizon by penalizing whenever there is deviation from desired behaviour. The advantage of using MPC lies in the fact that its cost function is capable of including multivariable terms which makes it a great asset to the control phenomenon. Even though this serves as an advantage it also means increasing the computational burden in the controller. The proposed control logic utilized the inductor current predicted values and devised a cost function such that it predicts and penalized future ripple magnitudes based on the system dynamics. The first term in Equation (29) tries to minimize the error and the second term in Equation (29) predicts and penalized the ripple at the next step (k+2) ensuring smooth transitions. The addition of the second terms ensures a good performance even under different load conditions such as RL loads.

$$G = \alpha\left(i_{L(ref)} - i_{L(k+1)}\right)^2 + \beta\left(i_{L(k+2)} - i_{L(k+1)}\right)^2 \tag{29}$$

where α and β are the weighing factors used for balancing different objectives.

**Table 1.** Comparison of traditional MPC current based cost functions

| Cost Function Type | Mathematical Expression | Effect on Performance |
|---|---|---|
| **Basic Current Tracking** | $G = \alpha\left(i_{L(ref)} - i_{L(k+1)}\right)^2$ | Good tracking but high ripple |
| **With Ripple Minimization (proposed)** | $G = \alpha\left(i_{L(ref)} - i_{L(k+1)}\right)^2 + \beta\left(i_{L(k+2)} - i_{L(k+1)}\right)^2$ | Smoother transitions and lower ripple |

Table 1 gives a comparison between traditional current tracking and the proposed current tracking in this work.

The design and selection of the weighting factors α and β in the cost function play a critical role in determining the performance and stability of the proposed predictive control strategy. Choosing inappropriate values can lead to poor prediction, increased ripple, or even instability in the control action. To address this, a simulation-driven sensitivity analysis was conducted to explore how different combinations of α and β affect system behavior under various operating conditions, including fluctuations in solar irradiance and load.

From this analysis, several key observations were made:

- A higher value of α gives more priority to accurate current tracking but also increases inductor current ripple.
- A higher value of β minimizes ripple but slows down the system's dynamic response.
- If the balance is not maintained, the system may either become oscillatory or too sluggish to respond to changes effectively.

Based on the trade-offs, the final values of α = 0.01 and β = 0.005 were selected, as they offered the best compromise between fast transient response, minimal ripple, and stable power output. These effects are visually represented in Figure 14, which illustrates how varying α and β values influence the cost function and overall converter performance.

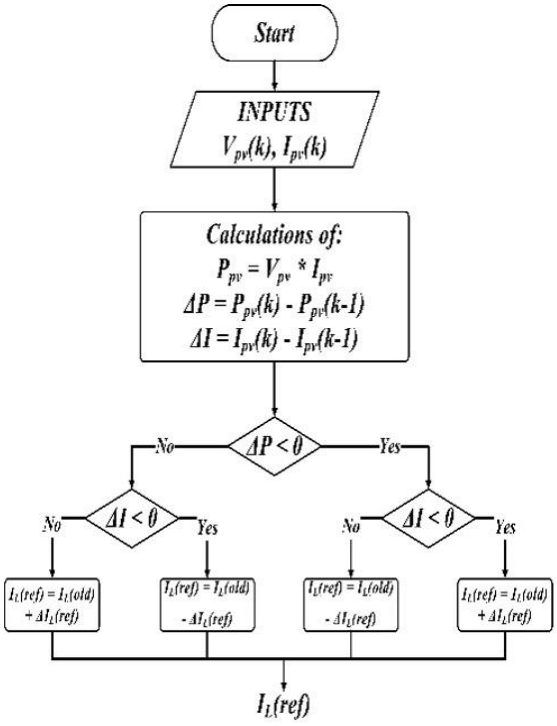


**Figure 6.** Algorithm for Perturb and Observe

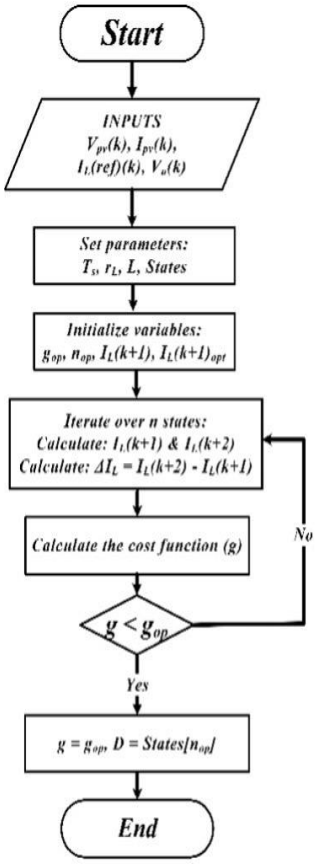


**Figure 7.** Algorithm for FCS-MPC

Although the selected values of α = 0.01 and β = 0.005 are not mathematically guaranteed to be globally optimal, they were found to be empirically effective across the

simulated operating conditions considered in this study. The tuning process was guided by sensitivity analysis, balancing the trade-off between current tracking accuracy and ripple minimization. Future research may explore automated parameter optimization using advanced techniques such as Bayesian optimization, genetic algorithms, or reinforcement learning. These approaches hold promise for real-time adaptation of the weighting parameters, potentially improving controller performance under highly dynamic and uncertain operating environments.

Figure 6 and Figure 7 explains workflow of the current tracking P&O algorithm and Finite Control Set MPC algorithm.

## 4. Simulation Results

Figure 8 provides a detailed overview of the control structure of the designed system. Table 2 and Table 3 presents solar module and boost converter parameters used for the validation of proposed PV system.

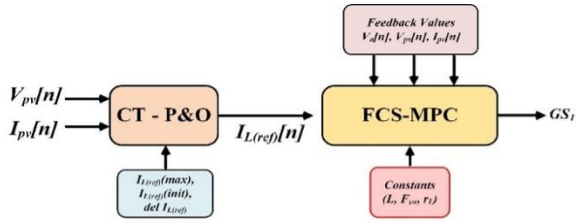


**Figure 8.** Detailed structure of the control strategy

**Table 2**. PV Module Data (1Soltech 1STH-215-P)

| Parameters | Values |
|---|---|
| Maximum Power, $P_{mpp}$ | 213.15 W |
| Open Circuit Voltage, $V_{oc}$ | 36.3 V |
| Short Circuit Current, $I_{sc}$ | 7.84 A |
| Voltage at maximum power point, $V_{mpp}$ | 29 V |
| Current at maximum power point, $I_{mpp}$ | 7.35 A |

Figure 9 and 10 represents the IV and PV characteristics of the solar cell from PV module and simulation results. The zoomed version in Figure 10 shows the effect of MPPT working.

**Table 3**. Boost Converter Parameters

| Parameters | Values |
|---|---|
| Inductance, $L$ | 9.26 mH |
| Capacitance, $C$ | 270 µF |
| Load Resistance, $R$ | 18.52 Ω |
| Ripple in inductor current, $\Delta i_L$ | 5 % |
| Ripple in capacitor voltage, $\Delta V_C$ | 1 % |

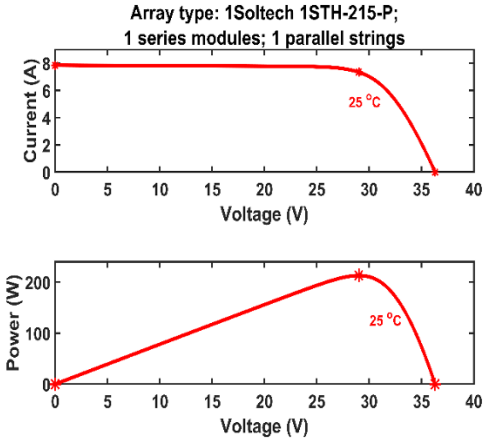


**Figure 9.** IV and PV characteristics from solar module

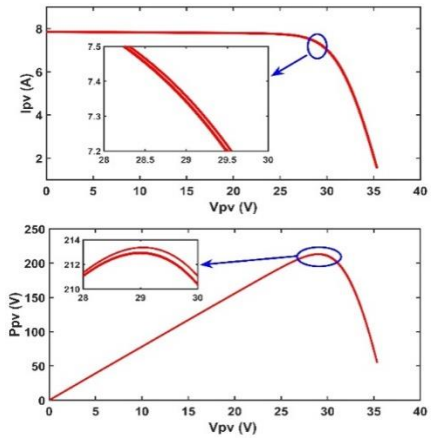


**Figure 10.** IV and PV characteristics (simulation)

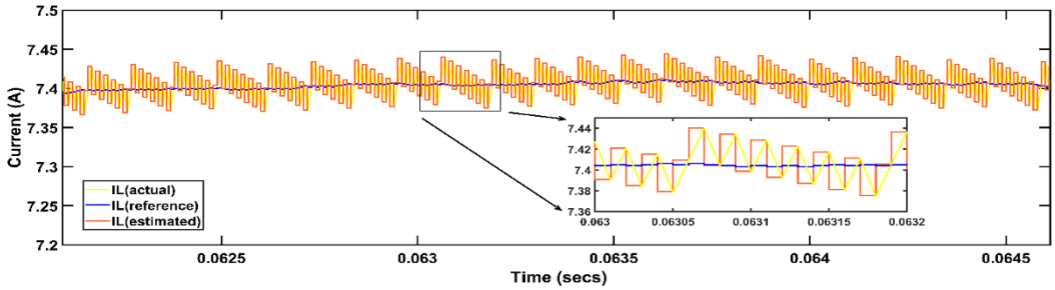


**Figure 11.** Waveforms of inductor current (actual, reference and estimated)

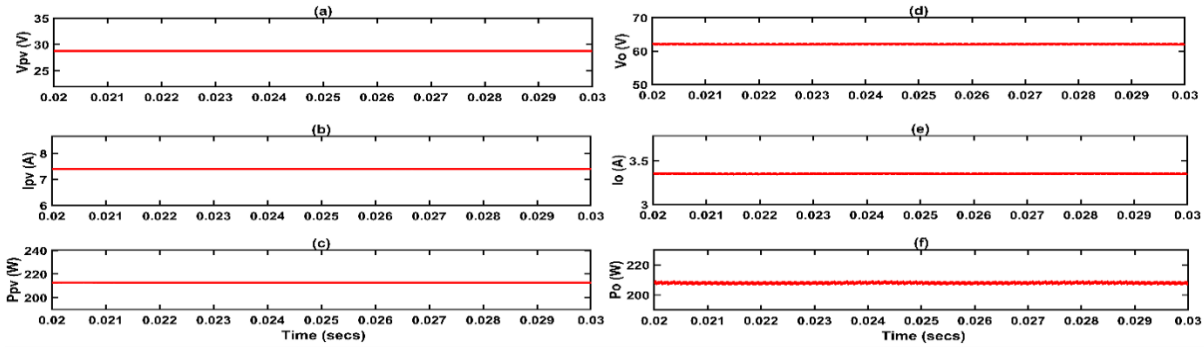


**Figure 12.** Waveforms of the PV and boost converter output. (a) PV voltage, (b) PV current, (c) PV power, (d) Output voltage, (e) Output current, (f) Output power.

The effectiveness of the proposed CT-P&O + FCS-MPC hybrid control strategy was validated through extensive simulations under both steady-state and dynamic conditions. This section walks through the results as presented sequentially from Figures 11 through 17. Figure 11 presents the actual, reference, and estimated inductor current waveforms under a constant irradiance of 1000 W/m². The steady-state inductor current reaches approximately 7.4 A, and the actual current closely tracks the reference. This illustrates the controller's ability to regulate the current precisely in real time, verifying that the predictive model functions as intended. In Figure 12, various PV-side and output-side parameters are shown. The average PV voltage stabilizes around 28.75 V—very close to the maximum power point voltage of 29 V—while the boost converter outputs a steady 62 V. The corresponding load current is about 3.35 A. From these values, the calculated input power is 212.8 W, and the output power is 208.1 W,

leading to an overall system efficiency of 97.8%. This highlights the controller's success in achieving effective MPPT while minimizing losses. Figure 13 illustrates the efficiency curve of the system under different load conditions. The consistency in efficiency across varying resistive loads further confirms the control strategy's adaptability and reliability in maintaining optimal performance, even when system demand changes. To assess the impact of cost function parameters, Figure 14 explores the effect of varying the weighting factors α and β. These parameters influence the balance between current tracking accuracy and ripple minimization. As shown, improper selection can degrade performance, while the chosen values (α = 0.01, β = 0.005) provide an optimal trade-off. This supports the tuning methodology discussed in Section 3.3.2. Figure 15 evaluates the system's behavior under a sudden load disturbance. A step change in load from 18.52 Ω to 9.26 Ω was applied at t = 0.1 seconds to simulate a 50% increase in current demand. The controller responded promptly, maintaining voltage and current stability with minimal transient effects. This demonstrates the system's robustness under abrupt and realistic changes in load. In Figure 16, the system's performance is tested with a resistive-inductive (RL) load to reflect more complex, non-linear real-world conditions, such as those introduced by motors or inductive appliances. Despite the presence of inductance, the proposed control scheme successfully regulates voltage, current, and power, confirming its ability to handle non-ideal load behaviors. Finally, Figure 17 depicts the system response under varying irradiance levels. The inductor current remains well regulated, and the control system continuously tracks the maximum power point, validating its effectiveness under environmental fluctuations. In summary, Figures 11 through 17 collectively demonstrate that the proposed hybrid controller is capable of high tracking accuracy, low ripple, and stable performance across a wide range of conditions. This includes steady-state operation, dynamic load variations, non-linear loads, and fluctuating irradiance—making it well suited for practical photovoltaic applications.

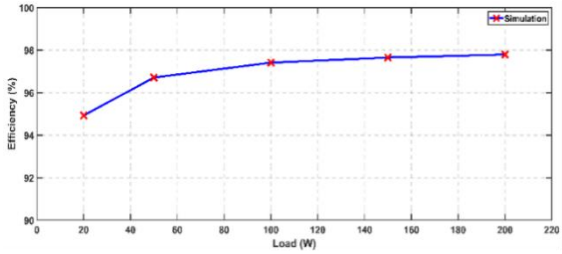


**Figure 13.** Efficiency curve

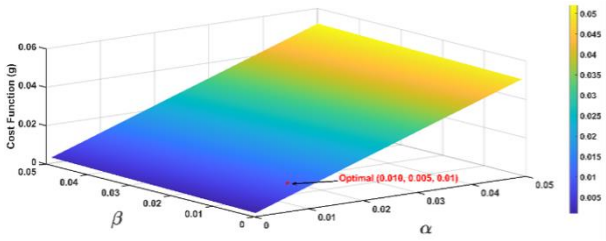


**Figure 14.** Effect of $\alpha$ and $\beta$ on cost function (g)

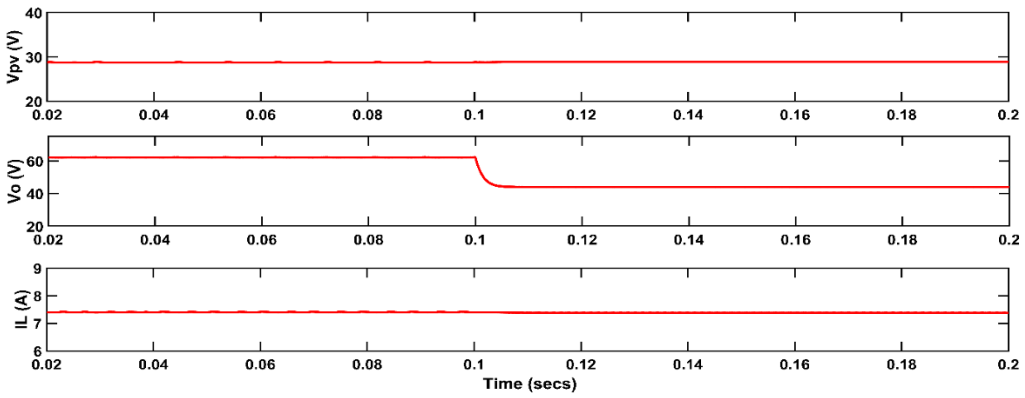


**Figure 15.** Dynamic change in load. At t = 0.1 sec the load is changed from 18.52 ohms to 9.26 ohms

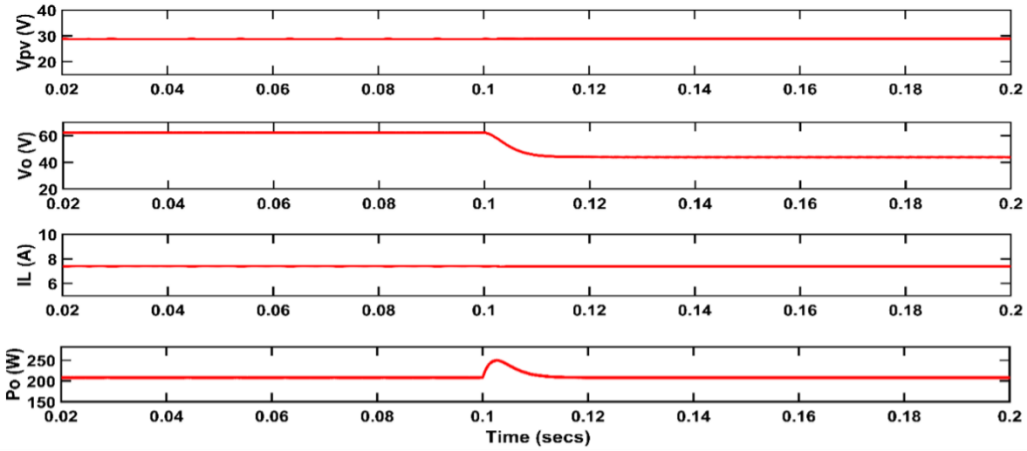


**Figure 16.** Effect on different parameters when load is changed from resistive to resistive-inductive load

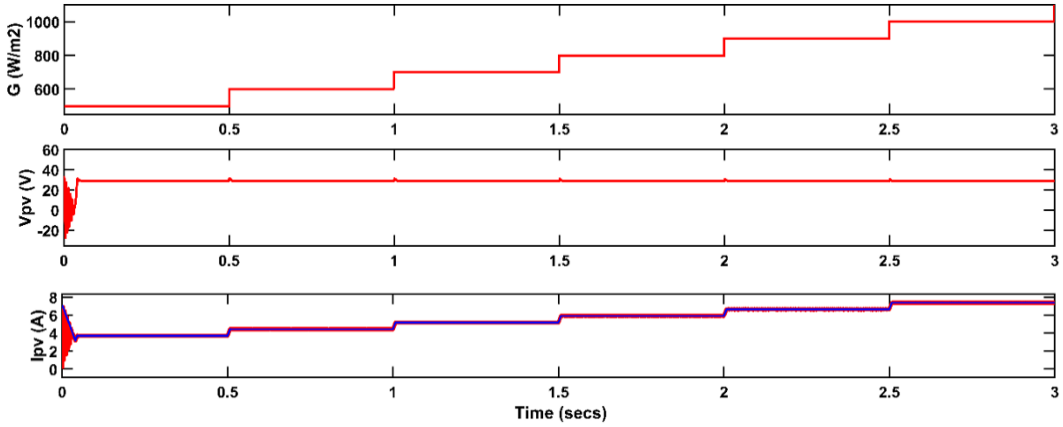


**Figure 17.** Dynamic change in insolation G ($W/m^2$)

## 7. Conclusions

This paper proposed a hybrid MPPT control technique that combines Current Tracking Perturb and Observe (CT-P&O) with Finite Control Set Model Predictive Control (FCS-MPC) to improve the performance of PV-fed boost converters. An enhanced cost function was introduced to reduce inductor current ripple while maintaining fast dynamic response and accurate current tracking. The system was validated through simulations under various conditions, including step changes in load, fluctuating irradiance, and both resistive and RL loads. Results confirmed stable operation and a high efficiency of 97.8%, demonstrating the controller's robustness and practical viability. Future work may focus on real-time implementation and adaptive parameter tuning using machine learning to further optimize performance in real-world applications.

## Multidisciplinary Domains

(a) Renewable and Sustainable Energy System, (b) Engineering needs for societal needs.

## Funding

This research received no external funding

## Conflicts of Interest

The author declares no conflict of interest

## Declaration on AI Usage

This article has been prepared without the use of AI tools.

## References

[1] Ellabban, O.; Abu-Rub, H.; Blaabjerg, F. Renewable energy resources: Current status, future prospects and their enabling technology. *Renew. Sustain. Energy Rev.* **2014**, *39*, 748–764, https://doi.org/10.1016/j.rser.2014.07.113.

[2] Esram, T.; Chapman, P.L. Comparison of Photovoltaic Array Maximum Power Point Tracking Techniques. *IEEE Trans. Energy Convers.* **2007**, *22*(2), 439–449, https://doi.org/10.1109/TEC.2006.874230.

[3] Liu, X.; Lopes, L. A. C. An improved perturbation and observation maximum power point tracking algorithm for PV arrays. *IEEE 35th Annual Power Electronics Specialists Conference (IEEE Cat. No.04CH37551)* 2004, 3, 2005-2010, https://doi.org/10.1109/PESC.2004.1355425.

[4] Hohm, D.P.; Ropp, M.E. Comparative study of maximum power point tracking algorithms. *Prog. Photovolt. Res. Appl.* 2003, *11*, 47–62, https://doi.org/10.1002/pip.459.

[5] Kouro, S.; Cortes, P.; Vargas, R.; Ammann, U.; Rodriguez, J. Model Predictive Control—A Simple and Powerful Method to Control Power Converters. *IEEE Trans. Ind. Electron.* **2009**, *56*(6), 1826–1838, https://doi.org/10.1109/TIE.2008.2008349.

[6] Rodríguez, J.; Cortés, P.; Silva, C.A. Predictive Control of Power Converters and Electrical Drives. In *Power Electronics and Motor Drives: Advances and Trends*, 2nd ed.

[7] Mohan, N.; Undeland, T.M.; Robbins, W.P**.** Power Electronics: Converters, Applications, and Design. In *Power Electronics: Converters, Applications, and Design*, 3rd ed.

[8] Jain, S.; Agarwal, V. Comparison of the Performance of Maximum Power Point Tracking Schemes Applied to Single-Stage Grid-Connected Photovoltaic Systems. *IEEE Trans. Energy Convers.* **2007**, *22*(3), 660–668, https://doi.org/10.1109/TEC.2006.874230.

[9] Salas, V.; Olias, E.; Barrado, A.; Lazaro, A**.** Review of the maximum power point tracking algorithms for stand-alone photovoltaic systems. *Sol. Energy Mater. Sol. Cells* **2006**, *90*(11), 1555–1578, https://doi.org/10.1016/j.solmat.2005.10.023.

[10] Hussain, A.; Sher, H.A.; Murtaza, A.F.; Al-Haddad, K**.** Revised Perturb and Observe Approach for Maximum Power Point Tracking of Photovoltaic Module Using Finite Control Set Model Predictive Control. *Proc. IEEE Int. Symp. Ind. Electron.* **2019**, 962–967, https://doi.org/10.1109/ISIE.2019.8781539.